Cosmic Masers: Proper Motion toward the Next-Generation Large Projects
Proceedings IAU Symposium No. 380, 2024
T. Hirota, H. Imai, K. Menten, & Y. Pihlström, eds.
doi:10.1017/S1743921323002259

Recombination lines and maser effects

Zulema Abraham[1]

[1]Instituto de Astronomia, Geofísica e Ciências Atmosféricas, Universidade de São Paulo
Rua do Matão 1226, CEP 05508-090, São Paulo, Brazil. email: zulema.abraham@iag.usp.br

Abstract. Maser effects occur in recombination lines when the plasma departs from local thermodynamic equilibrium (LTE). Its consequence is not as dramatic as that found in molecular masers, and therefore it is more difficult to recognize. Besides, it occurs in compact high density regions, and its lines fall at millimeter and submillimeter wavelengths, only recently available with good angular resolution. This review will focus on the theoretical aspects of maser recombination lines and on the recent detection of these masers in different astronomical objects.

Keywords. masers, radio lines, stars: mass loss, HII regions, jets and outflows

1. Introduction

Radio recombination lines are the result of transitions between atomic energy levels of high quantum number n. The electrons populate these levels after recombination, and then decay into lower levels, producing the lines.

The first recombination line (H90α) towards HII regions was detected at cm wavelengths in 1964 from Pushchino (Dravskikh & Dravskikh 1964) and in 1965 (109α) from NRAO (Hoglund and Mezger 1965). During the first years, the velocity measured from the radio recombination lines was used to study the spiral structure of our Galaxy.

The intensity of the recombination lines, together with that of the bremsstrahlung continuum radiation was used to determine the physical conditions of the clouds (density and temperature) assuming local thermodynamic equilibrium (LTE) conditions of the gas. It was soon seen that the temperatures obtained from radio recombination lines in large HII regions were smaller than those obtained from optical lines (eg. Mezger and Hoglund 1967). The reason could be inhomogeneity in the temperature distribution or the assumption of LTE not being valid, implying maser effects (Goldberg 1966).

The discovery of the first maser in recombination lines occurred in 1989 in the massive star MCW349A (Martin-Pintado *et al.* 1989) and later in the massive and evolved star η Carinae (Cox *et al.* 1995).

At the time of our last maser meeting in Cagliari, other maser candidates were reported: the source IRS2 in MonR2 (Jiménez-Serra *et al.* 2020), and later the Planetary Nebula Mz3, in data obtained with Hershel (Aleman *et al.* 2018).

The question is why it took so long for these discoveries, and the answer is that it was necessary to look at the right lines and the right objects.

2. Recombination Line Maser Theory

The discovery of masers in recombination lines led to the study of the physical conditions necessary for maser amplification. The first comprehensive study was presented by Strelnitski *et al.* (1996). He considered the radiative transfer across a plane parallel slab of width s.

The equation of radiative transfer can be written as:

$$\frac{dI_\nu}{d\tau_\nu} = -I_\nu + \frac{j_\nu}{\kappa_\nu}, \tag{2.1}$$

where I_ν is the specific intensity at frequency ν (energy of the radiation per unit surface, time, frequency and solid angle), j_ν is the emission coefficient, κ_ν the absorption coefficient per unit length, and τ_ν the optical depth, given by:

$$\tau_\nu = \int_0^s \kappa_\nu \, ds. \tag{2.2}$$

The solution of equation 2.1 is:

$$I_\nu = I_\nu(0)e^{-\tau_\nu} + S_\nu\left[1 - e^{-\tau_\nu}\right], \tag{2.3}$$

with:

$$S_\nu = \frac{j_\nu}{\kappa_\nu}. \tag{2.4}$$

S_ν is called the source function and in thermodynamic equilibrium is equal to the Planck function $B_\nu(T)$. In general, the source function contains all the physics: scattering, stimulated emission, non-uniformity, etc.

Let us consider no background radiation, and transition between two levels $n_1 \rightarrow n_2$ along a slab of depth L. The source function can be written as:

$$S_\nu = \eta_\nu B_\nu(T), \tag{2.5}$$

with:

$$\eta_\nu = \frac{\kappa_c^* + \kappa_L^* b_2}{\kappa_c^* + \kappa_L^* b_1 \beta_{12}}, \tag{2.6}$$

and

$$\beta_{12} = \frac{1 - \frac{b_2}{b_1}\exp(-h\nu_0/kT_e)}{1 - \exp(-h\nu_0/kT_e)}, \tag{2.7}$$

b_n represents the population of the level of quantum number n relative to its LTE value, β_{12} is the ratio between the correction factor for stimulated emission and its LTE value and ν_0 is the rest frequency of the transition.

The level population of the H atoms, relative to their LTE values was calculated with different degrees of accuracy. Initially, only the quantum number n was considered (Brockelhurs 1970, Walmsley 1990). Storey & Hummer (1995) included later the angular momentum l, and finally the contribution of the continuum radiation was introduced (Prozesky A. & Smits 2018, Zhu *et al.* 2019).

Depending on the ratio b_2/b_1, β_{12} can be negative. The same is valid for η_ν, which also depends on value of the absorption coefficients, which can be written as:

$$\kappa_c^* = 6.64 \times 10^{-8} \frac{N_e N_1}{\nu^2} \left(\frac{10^4}{T_e}\right)^{1.5} g_{\rm ff} \quad {\rm pc}^{-1}, \tag{2.8}$$

$$\kappa_L^* = 1.06 \times 10^{12} \frac{N_e N_i(v)}{\nu} \left(\frac{10^4}{T_e}\right)^{2.5} mK(m) \exp\left(\frac{\xi_n}{kT_e}\right)(\nu\phi_\nu), \tag{2.9}$$

N_e and N_i are the electron number density of electrons and ions, respectively, T_e the electron temperature, $g_{\rm ff}$ the Gaunt factor for continuum bremsstrahlung, $mK(m)$ is an approximation to the oscillator strength given by Menzel (1968), ξ_n the energy of level n

https://doi.org/10.1017/S1743921323002259 Published online by Cambridge University Press

and $\phi(v)$ the line profile, which takes into account the Doppler, turbulence and pressure broadening.

The total optical depth of the slab to radiation of frequency ν is:

$$\tau_{tot} = \tau_c + \tau_L = (\kappa_c^* + \kappa_L^* b_1 \beta_{12}) L \tag{2.10}$$

The intensity at the line center, relative to the continuum is expressed by:

$$r(\nu_0) = \frac{I(\nu_0) - I_c(\nu_0)}{I_c(\nu_0)} = \eta \frac{1 - \exp(-\tau_{tot})}{1 - \exp(-\tau_c)} - 1, \tag{2.11}$$

or

$$r(\nu_0) = \eta \frac{1 - \exp(-\tau_c - \tau_L)}{1 - \exp(-\tau_c)} - 1 \tag{2.12}$$

Depending on the sign of η and the relative values of τ_c and τ_L we can have different values for $r(\nu_0)$. In particular, when η and τ are large and negative,

$$r(\nu_0) \approx \frac{|\eta|}{1 - \exp(-\tau_c)} \exp(|\tau_{tot}|). \tag{2.13}$$

Note that η depends only on the physical conditions of the emitting region, while the optical depth depends on the velocity distribution of the material, implying that the length L can be different for the continuum and for the line, which requires frequency coherence.

Since τ_{tot} is negative, and it is formed by the sum of τ_c and τ_L, there will be a large difference between the intensity of the recombination lines when the region becomes optically thin, as observed in MCW349A, between the lines H41α and H30α.

3. Maser Recombination Lines in η Carinae

η Carinae (hereafter η Car) is the object that presents the strongest recombination line masers detected until now (Cox *et al.* 1995, Abraham *et al.* 2014, 2022). The star, which possibly is in the LBV (Luminous Blue Variable) phase of evolution, underwent a strong episode of mass loss (> 30 M$_\odot$) in 1840; the ejected mass expanded, cooled down and formed the well-known Homunculus Nebula. η Car is part of a binary system in an extremely eccentric orbit, with period of 5.52 years, as revealed by the strictly periodic light curves, observed from radio frequencies to X-ray energies (Damineli 1996, Corcoran *et al.* 2017). The companion star, as well as the photosphere of η Car are not directly visible, because they are embedded in the massive slow wind of η Car, but the companion (probably a Wolf-Rayet star) is believed to have a fast wind of its own; the wind-wind collisions produce shocks that are the origin of the X-ray emission.

Interferometric observations of the binary system at cm wavelengths obtained with the Australian Compact Array (ATCA) revealed extended continuum emission from the surroundings of the binary system, coincident with the Homunculus Nebula, and a disk like structure at the core, with an extension and intensity that varied with the phase of the binary orbit (Duncan & White 2003). This structure was interpreted as gas ionized by the hot companion star, which provided a number of ionizing photons that varied with the orbital phase.

Although cm wave recombination lines were also observed together with the continuum emission, only mm wave lines, observed with the SEST radiotelescope with arcsec resolution, presented strong maser effects, first attributed to the dense wind of η Car (Cox *et al.* 1995). These maser sources presented a single line, contrary to what is observed in the other maser sources, which were modeled as a combination of a Keplerian disk and wind ejected from the disk (Báez-Rubio *et al.* 2013, Jiménez-Serra *et al.* 2020).

https://doi.org/10.1017/S1743921323002259 Published online by Cambridge University Press

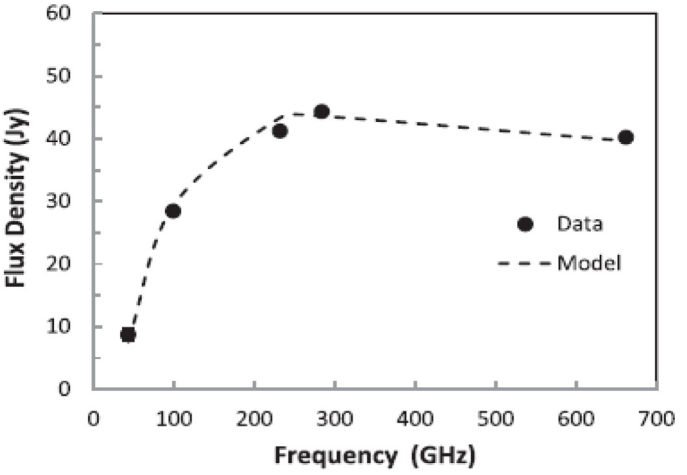

Figure 1. Continuum pectrum of η Car obtained with ALMA on 2014 (Abraham *et al.* 2014).

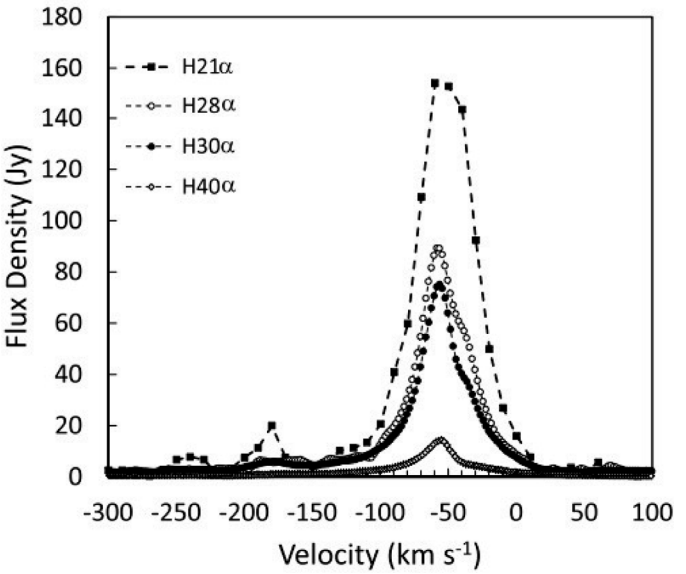

Figure 2. Recombination line spectra of η Car obtained with ALMA on 2014 (Abraham *et al.* 2014).

η Car was observed with ALMA on 2012 (cycle 0) in the recombination lines H42α, H40α, H30α, H28α, and H21α (Abraham *et al.* 2014), but it was not resolved, even at the higher frequencies, where the beam size was 0.35×0.42 arcs (at the distance of η Car 50 mas correspond to 110 au).

The continuum spectrum is compatible with that of an HII region, with a turnover frequency close to 300 GHz, as can be seen in Figure 1.

In Figure 2 we show the superimposed spectra of the H40α, H30α, H28α, and H21α lines.

Based on the cm wave observations, which were modeled as originated in an expanding source, the mm wave continuum and lines were modeled as arising from an expanding shell of radius $R = 6.6 \times 10^{15}$ cm, width $\Delta R = 0.1R$, electron density $N_e = 1.3$ km s^{-1} and temperature $T_e = 1.7 \times 10^4$ K, expanding with a bulk velocity of 53 km s^{-1}, with

https://doi.org/10.1017/S1743921323002259 Published online by Cambridge University Press

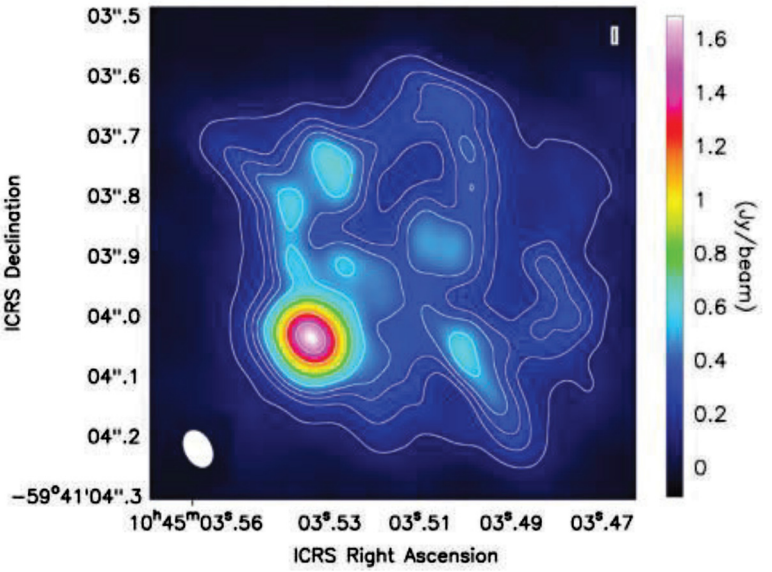

Figure 3. 230 GHz continuum image of η Car obtained with ALMA on 2017 (Abraham *et al.* 2020).

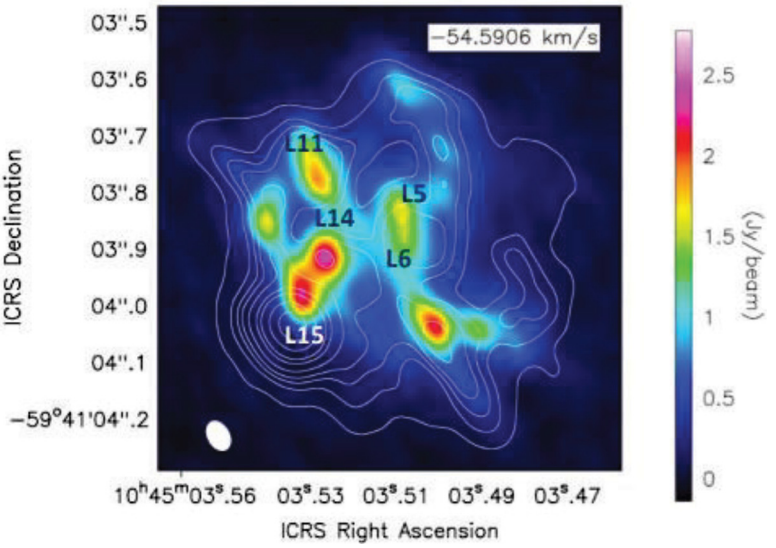

Figure 4. Iso-velocity image of the recombination line H30α, centered at the velocity of -54.6 km s^{-1} and resolution of 1.3 km s^{-1}, of η Car obtained with ALMA on 2017 (Abraham *et al.* 2020).

the velocity ranging from 60 km s^{-1} to 20 km s^{-1} in the inner and outer borders of the shell, respectively.

However, η Car was observed again with ALMA in the 230 GHz continuum and in the H30α recombination line on 2017, with resolution 65 × 43 mas, and the expanding shell model was not confirmed.

In fact, the continuum emission showed a compact source, centered on η Car and extended emission in the NW direction, as can be seen in Figure 3.

https://doi.org/10.1017/S1743921323002259 Published online by Cambridge University Press

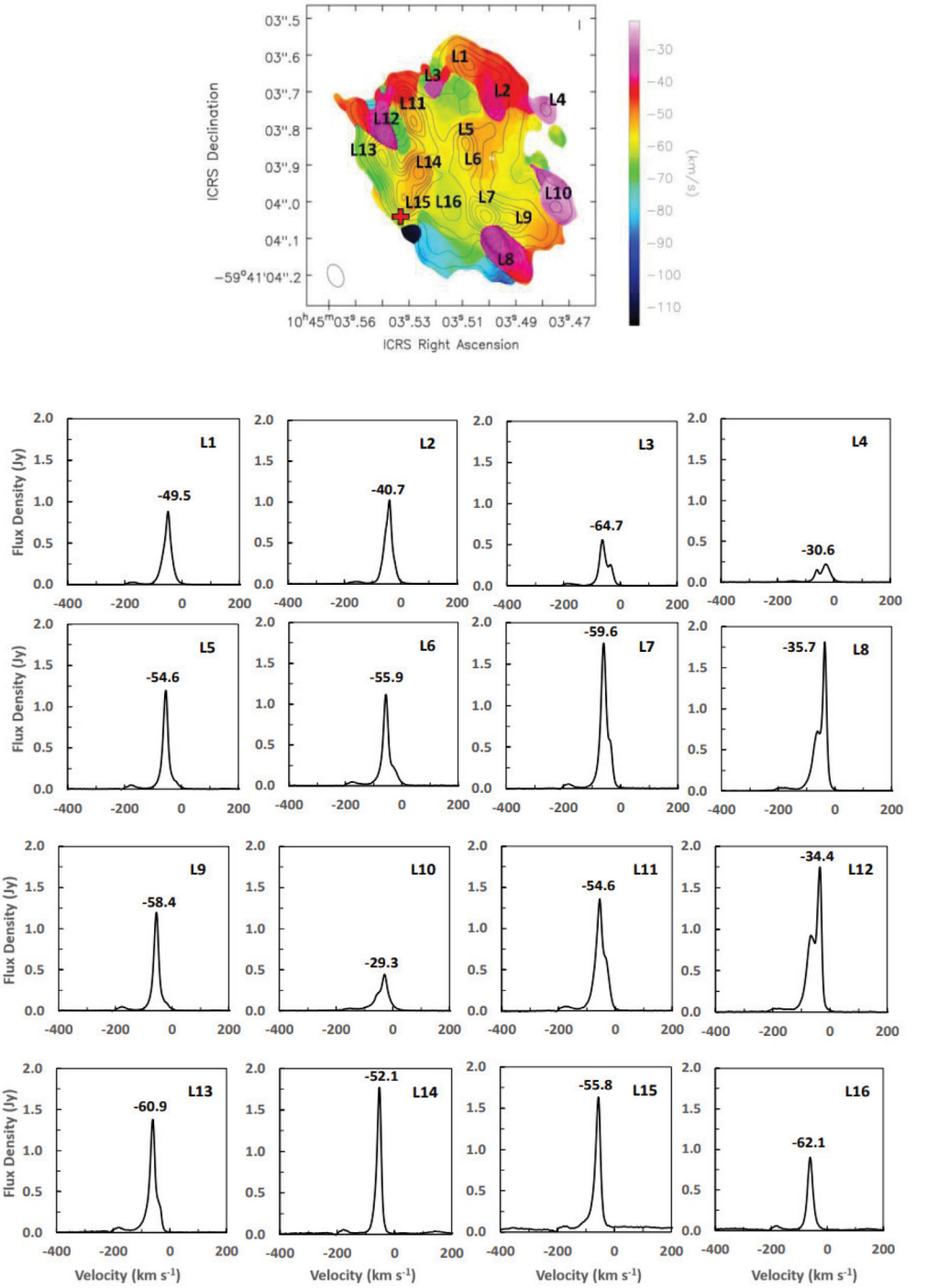

Figure 5. Spectra of the 16 compact component identified in the H30α images of η Car detected with ALMA in 2017. (Abraham *et al.* 2020).

https://doi.org/10.1017/S1743921323002259 Published online by Cambridge University Press

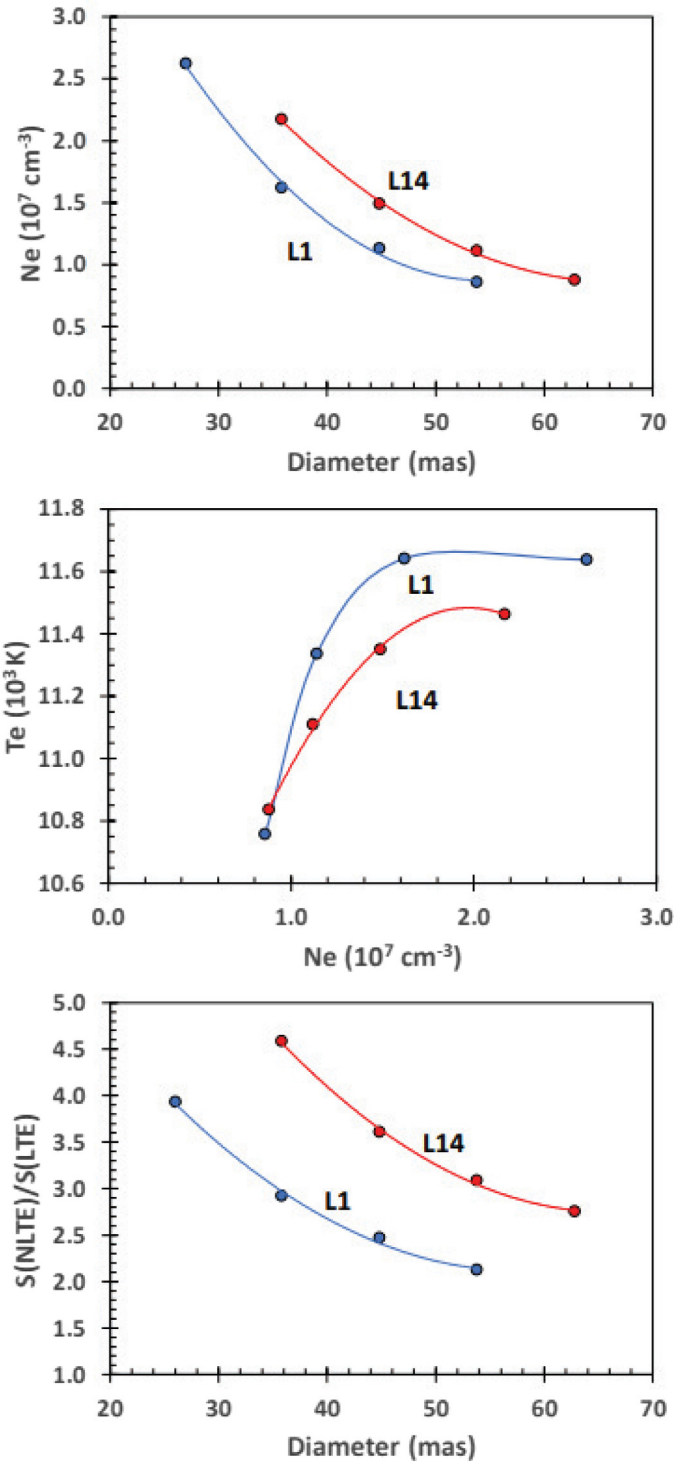

Figure 6. Physical conditions of the clumps that fit the spectra of the H30α recombination line of clumps 1 and 14, as identified in Figure 5.

https://doi.org/10.1017/S1743921323002259 Published online by Cambridge University Press

The iso-velocity intensity maps of the different velocity channels, with width of 1.3 km s^{-1}, revealed several compact (not resolved) components with different velocities on top of the 230 GHz continuum emission. One of these maps, centered at the velocity of maximum emission is shown in Figure 4.

In Figure 5 we show the profiles of the different clumps, identified in the image of the first intensity momentum superimposed on the raster image of the line velocity. We can see that the positions and velocities of the clumps are not compatible with the model of an expansion shell.

Since the maser sources are not resolved, the physical conditions of two of them, labeled as 1 and 14, were investigated for different values of the radius (smaller than 50 mas or 110 ua), assumed to be spherical and homogeneous clumps. The results are shown in Figure 6.

References

Abraham, Z., Beaklini, P. P. B., Cox, P., *et al.* 2020, *MNRAS*, 499, 2493
Abraham, Z., Falceta-Gonçalves D., Beaklini P. P. B., 2014, *ApJ*, 791, 95
Abraham Z., Beaklini P. P. B., Cox, P., Falceta-Gonçalves D., Nyman L-A, 2020, *MNRAS*, 499, 2493
Aleman, I. *et al.* 2018, *MNRAS*, 477, 4499
Bez-Rubio, A., Martn-Pintado J., Thum C., Planesas P., 2013, *A&A*, 553,45
Brockelhurst, M. 1979, *MNRAS*, 148, 417
Corcoran, M. F., Liburd, J., Morris, D., *et al.* 2017, *ApJ*, 838, 45
Cox P. *et al.* 1995, *A&A*, 295, L39
Damineli, A. 1996, *ApJ*, 460, L49
Dravskikh, Z. V. & Dravskikh, A. F., 1964, *Astron. Tsirk.*, 282, 2
Duncan, R. A., White, S. M., 2003, *MNRAS*, 338, 425
Goldberg, L., 1966, *ApJ*, 144, 1225
Hoglund, B. and Mezger, P. G., 1965, *Science*, 150, 339.
Jimnez-Serra, I., Bez-Rubio, A., Martn-Pintado, J., Zhang, Q., Rivilla, V. M., 2020, *ApJ*, 897, 33
Martin-Pintado, J., Bachiller, R., Thurn, C., Walmsley, C. M., 1989, *A&A*, 215, L13
Menzel, D. H., 1968, *Nature*, 218, 756.
Mezger, P. G. & Hoglund, B., 1967, *ApJ*, 147, 579
Prozesky, A. & Smits, D. P., 2018, *MNRAS*, 478, 2766
Storey, P. J., Hummer, D. G., 1995, *MNRAS*, 272, 41
Strelnitski, V. S., Ponomarev, V. O., Smith, H. A. 1996, *ApJ*, 470, 1118
Walmsley, C. M. 1990, *A&AS*, 82, 201
Zhu, F.-Y., Zhu, Q.-F., Wang, J.-Z., Zhang, J.-S., 2019, *ApJ*, 881, 14

https://doi.org/10.1017/S1743921323002259 Published online by Cambridge University Press